RSC Advances

PAPER

View Article Online
View Journal | View Issue

Cite this: *RSC Adv.*, 2018, **8**, 1677

Engineering stem cell-derived 3D brain organoids in a perfusable organ-on-a-chip system†

Yaqing Wang,[acd] Li Wang,[a] Yaqiong Guo,[ac] Yujuan Zhu[ac] and Jianhua Qin *[abc]

Brain organoids derived from the self-organization of human induced pluripotent stem cells (hiPSCs) represent a new class of *in vitro* organ system for modeling brain development and diseases. However, engineering brain organoids in a biomimetic environment that is favorable for brain development remains challenging. In this work, we present a new strategy to generate hiPSCs-derived 3D brain organoids using an organ-on-a-chip system in a controlled manner. This system provides a biomimetic brain microenvironment by incorporating three-dimensional (3D) Matrigel, fluid flow and multicellular architectures of tissues that allows for extended 3D culture, *in situ* neural differentiation, and organization of brain organoids on a single device. The generated brain organoids display well-defined neural differentiation, regionalization and cortical organization under perfused culture conditions, which recapitulate the key features of early human brain development. Moreover, the brain organoids exhibit an enhanced expression of cortical layer markers (TBR1 and CTIP2) under perfused cultures as compared to that under static cultures on a Petri dish, indicating the role of mechanical fluid flow in promoting brain organogenesis. The simple and robust brain organoids-on-a-chip system may open new avenues for various stem cell-based organoids engineering and its application in developmental biology and human disease studies.

Received 23rd October 2017
Accepted 23rd December 2017

DOI: 10.1039/c7ra11714k

rsc.li/rsc-advances

Introduction

The great advances in human pluripotent stem cells (PSCs) have enabled the generation of *in vitro* 3D cellular clusters *via* self-renewal and self-organization of stem cells, termed organoids.[1–3] The organoid models are capable of reproducing specific features of native tissues or organs with remarkable similarity in terms of cell type complexity, architecture and functions, bridging the gap between animal studies and traditional 2D culture models.[2,3] Because organoids can be grown from human stem cells and patient induced PSCs, they hold great promise for modeling organ development, studying the mechanisms of human diseases and drug discovery.[4,5] Recently, several researchers have reported the successful generation of various human organoids for delineating the physiological characteristics of human developing organs, such as the brain, liver and intestine.[6–9] Among these organoids, brain organoids exhibit the most complicated and organizational patterns with distinct brain regions and cortical structure, demonstrating their great potential to facilitate the investigation of various aspects of human brain development and disease pathology *in vitro*.[10–14]

At present, brain organoids are commonly generated *via* self-renewal and self-organization of PSCs in 3D culture.[6,7,15] Typically, the multicellular aggregates from stem cells, called embryoid bodies (EBs), are initially encapsulated into Matrigel for 3D culture and neuroepithelial expansion.[16] Then, the EBs were transferred into Petri dishes or spinning bioreactors for suspended culture and generation of brain organoids. *In vivo*, brain development is characterized by a dynamic and protracted process beginning with early gestation.[17] Actually, tissue morphogenesis and organogenesis in the developing embryo are tightly regulated by the stem cell microenvironment they foster, which contains a series of factors including mechanical fluid flow and intrinsic or extrinsic biochemical signals.[18,19] Although stem cell-derived organoids recapitulate the early developmental process of organs, differences from the native organs still exist, which suggest that the microenvironment factors, such as biochemical, physical signals and multicellular interactions are either lacking or presented incorrectly. Moreover, the current approaches for organoid formation are limited by the risk of contamination due to multiple steps, necessity for large volumes of culture media, and complicated instruments with high cost.

The emerging organs-on-a-chip are biomimetic 3D microsystems stemmed from microfluidic technology, which aim to

[a]*Division of Biotechnology, Dalian Institute of Chemical Physics, Chinese Academy of Sciences, 457 Zhongshan Road, Dalian 116023, China. E-mail: jhqin@dicp.ac.cn; Fax: +86-411-84379059*

[b]*Center for Excellence in Brain Science and Intelligence Technology, Chinese Academy of Sciences, Shanghai, China*

[c]*University of Chinese Academy of Sciences, Beijing 100049, China*

[d]*Key Laboratory of Separation Sciences for Analytical Chemistry, Dalian Institute of Chemical Physics, Chinese Academy of Sciences, China*

† Electronic supplementary information (ESI) available. See DOI: 10.1039/c7ra11714k

recreate the minimal functional units of living organs by replicating the key structural and physiological features.[20–22] Organs-on-a-chip can mimic the *in vivo*-like cellular microenvironment and organ level functions by precisely controlling over the related factors such as fluid flow, cell–cell and cell–matrix interactions, mechanical forces and biochemical cues.[23–25] Presently, the miniaturized models of several organs, including lungs,[24] liver,[25] intestine[26] and neural networks[27] have been created. Although several work have reported the culture of hiPSCs-derived tissue specific cells on the organ-on-a-chip systems,[25,28,29] to our knowledge, no work has been devoted to the engineering of hiPSCs-based brain organogenesis in perfused 3D culture using these systems.

In this study, we proposed a new strategy to engineer 3D brain organoids derived from hiPSCs by combining stem cell biology with organs-on-a-chip technology. The established brain organoids-on-a-chip system enabled hiPSCs-based EBs culture, *in situ* neuronal differentiation and formation of brain organoids by incorporating self-organization of brain tissues, 3D Matrigel and fluid flow. The expressions of neural markers (Nestin, SOX2 and TUJ1), brain regional markers (PAX6, PAX2 and ISL1) and cortical layer markers (TBR1 and CTIP2) in brain organoids were identified. The comparisons of neural differentiation and the cortex specific genes expression under chip-based perfused culture and static cultures on Petri dish were evaluated as well.

Materials and methods

Fabrication of the brain organoids-on-a-chip device

The brain organoids-on-a-chip device was fabricated using a conventional soft lithography procedure and was made of polydimethylsiloxane (PDMS, from Dow Corning Corp). The masks were designed by AutoCAD and printed on plastic film. To fabricate the template, SU-8 3050 negative photoresist (MicroChem Corp) was spin-coated onto the clean glass and then selectively cured under ultra violet light source with masks. The chip contained two layers: top and bottom. The top layer consisted of two parallel culture chambers and three separate medium channels. The height of the top layer channels was approximately 600 μm. Two parallel culture chambers (width: 2.5 mm; length: 14 mm) were separated by a central channel (width: 1 mm; length: 20 mm), which contained 10 trapezoid pillar array structures at both sides of the channel for interconnection (ESI Fig. S1†). The two parallel chambers were used for the 3D culture and formation of brain organoids. The central channel served as the fluid flow passageway, with inlet and outlet holes of 0.8 mm in diameter created with a sharp needle. The channels at the two sides of the device were filled with cell culture medium. The bottom layer of the device was the plane PDMS layer. The top and bottom layers were molded by the PDMS pre-polymer containing a 10 : 1 (w/w) mixture of the PDMS precursor and curing agent. The pre-polymer in the channels was then polymerized by thermal curing in 80 °C dry oven for 1 h. Next, the top layer of the chambers was adhered to the plane PDMS layer after a 90 s oxygen plasma treatment (plasma power: 200 W, O_2 pressure: 0.2 MPa). Finally, the devices were autoclaved to restore the hydrophobicity of PDMS and were kept sterile until use.

Evaluation of substance distribution on chip

The validation of substance distribution across the 3D Matrigel was performed by sodium fluorescein permeation assay. Hydrophilic sodium fluorescein tracer (NaFI, 376 Da) diluted in phosphate buffered saline (PBS) at a ratio of 1 : 1000 was introduced into the central fluidic channel using a syringe pump. The fluorescent images were obtained under static or 25 μl h^{-1} flow rate conditions at given time intervals. Images were analyzed using ImageJ (NIH) to plot the intensity profiles.

Generation of EBs

EBs are the 3D multicellular aggregates from the hiPSCs *via* 3D culture. The hiPSCs derived from skin fibroblasts (provided as a gift from Dr Ning Sun) were cultured in mTeSR1 medium on six well plates each coated with 1.5% Matrigel (BD Biosciences) in DMEM/F12 medium (Invitrogen). The medium was changed daily. Cells were passaged at a 1 : 5 ratio by digestion with Accutase (Sigma-Aldrich) until achieved 75–90% confluence. The pluripotency of the hiPSCs was regularly verified by cell morphology and immunostaining for the pluripotent markers.

Knockout serum replacement (KSR) medium was prepared using DMEM/F12 medium supplemented with 20% KSR (Invitrogen), 1% GlutaMAX (Invitrogen), 1% minimum essential media-nonessential amino acids (MEM-NEAA, Invitrogen), 0.2 mM 2-mercaptoethanol (Sigma-Aldrich) and 1% penicillin–streptomycin (Sigma). Dissociated hiPSCs ($\sim 5 \times 10^6$ cells) were resuspended in KSR medium and immediately added to 10 μM ROCK inhibitor Y27632 (Millipore) and a low concentration of basic fibroblast growth factor (bFGF, 4 ng ml^{-1}, Peprotech). The cells were then seeded in concave wells (diameter: 800 μm) for the EB formation. The generated EBs were 100–300 μm in diameter. The EBs were then transferred into a low-adhesion plate, and fresh KSR medium was changed every other day. At day five, the KSR medium was replaced with neural induction medium (NIM) that contained DMEM/F12, 1% GlutaMAX, 1% MEM-NEAA, 1 μg ml^{-1} heparin (Sigma), 1% N2 supplement (Invitrogen) and 1% penicillin–streptomycin. The EBs were then cultured for another six days with NIM.

Perfused culture of the EBs on chip

Neural differentiation medium (NDM) was prepared using a mixture of DMEM/F12 and Neurobasal medium (Invitrogen) at a volume ratio of 1 : 1, supplemented with 1% B27 supplement, 0.5% N2 supplement, 0.2 mM 2-mercaptoethanol, 1% GlutaMAX, 0.5% MEM-NEAA and 1% penicillin–streptomycin. At day 11, approximately 300 EBs per milliliter were suspended within ice-cold Matrigel. Next, 40–50 μl of the EB-Matrigel mixture was carefully pipetted into each hydrogel channel of the chip. The chip was then incubated at 37 °C for 25–30 min to make Matrigel gelation. The EBs were immobilized into the Matrigel and aligned in the channels of the chip. A flexible polytetrafluoroethylene (PTFE) tube was connected to the inlet of the central medium channel; this set-up provided

a continuous flow of NDM at the rate of 25 μl h^{-1} using a syringe pump system. In addition, the spheroids were cultured on chip under static conditions as the control group from day 11 to day 33 and the media were changed twice every day for sufficient media supplement. In conventional Petri dish cultures, EBs were embedded in Matrigel droplet at day 11 and floating cultured in low-adhesive Petri dish. The 50% of media volume was exchanged every day for up to three weeks.

Cryosection and immunohistochemical staining

In order to precisely reveal the detailed characterizations of brain organoids by immunohistochemical staining, brain organoids were retrieved from the chip by gently mechanically splitting the chip layers on desired days during the development period. Brain organoids were fixed in 4% paraformaldehyde (PFA) for 25–30 min at room temperature. The fixed organoids were then washed in PBS three times, transferred to 30% sucrose solution and incubated at 4 °C overnight. Subsequently, the dehydrated tissues were embedded in O.C.T. compound (SAKURA), snap frozen and stored at −80 °C. For immunofluorescence staining, 10 μm thick sections were obtained with a cryostat (Leica). Cryosections with samples on adhesive slides were washed in PBS to remove excess O.C.T. and permeabilized with 0.25% Triton X-100 diluted in PBS for 5 min at room temperature. Then, the sections were blocked with 10% goat serum (Solarbio, SL1) for one hour. Next, the sections were incubated overnight at 4 °C with a primary antibodies diluent. The following primary antibodies were used for immunohistochemistry: TUJ1 (mouse, 1 : 500, BioLegend 801201), PAX6 (rabbit, 1 : 300, BioLegend PRB-278P), PAX2 (mouse, 1 : 500, Abnova H00005076-M01), SOX2 (rabbit, 1 : 500, Cell Signaling 3579), Nestin (mouse, 1 : 500, Santa Cruz sc-20978), CTIP2 (rat, Abcam ab18465, 1 : 500), TBR1 (rabbit, Abcam ab31940, 1 : 200), CD133 (rabbit, Bioss, bs-4770R, 1 : 100), ISL1 (mouse, Thermo MA5-15515, 1 : 100). Samples were washed with PBS three times to remove excess primary antibodies and were then incubated with secondary antibodies Alexa Fluor 488 or 594 dyes (1 : 100) for one hour at room temperature. Nuclei were then counterstained with 4′,6-diamidino-2-phenylindole (DAPI, Life technologies, 1 : 4000) for 15 min. All images were photographed using a confocal microscope (Olympus). ImageJ (NIH) was used to merge images and to uniformly adjust the brightness or contrast. Image-Pro Plus was used to assess and quantify the fluorescence intensity of the expression of specific markers under identical settings.

TUNEL assay

The apoptosis of cells within EBs was assessed by TUNEL assay after 33 days of culture in the brain organoids-on-a-chip system. Tissue cryosections were treated by TUNEL kit reagents (Life Technologies) according to the manufacturer's instructions. After incubation with staining reagents, the samples were washed three times with PBS, and images were acquired using a confocal microscope. The viability of cells was quantitatively analyzed by using ImageJ (NIH) to calculate the percentage of TUNEL positive cells.

Real-time PCR

Total mRNAs were isolated from the whole brain organoids or hiPSCs using Trizol reagent (TAKARA) and the final concentration was adjusted to 250 ng μl^{-1}. The RNA concentration and quality were determined using Nano Drop (Thermo Fisher Scientific). The cDNA was then produced and amplified using Ex Taq DNA polymerase (TAKARA) under the following reaction conditions (35 cycles): denaturation at 95 °C for 1 min, annealing at 58 °C for 30 s, and extension at 72 °C for 30 s. The primer pairs used were as follows: OCT4 forward: 5′-GGA GAA GCT GGA GCA AAA CC-3′, reverse: 5′-TGG CTG AAT ACC TTC CCA AA-3′; SOX1 forward: 5′-TAT CTT CTG CTC CGG CTG TT-3′, reverse: 5′-GGG TCT TCC CTT CCT CCT C-3′; PAX6 forward: 5′-AGT TCT TCG CAA CCT GGC TA-3′, reverse: 5′-ATT CTC TCC CCC TCC TTC CT-3′; PAX2 forward: 5′-CTG GGC AGC AAC GTG TCA-3′, reverse: 5′-GAG TGG TGC TCG CCA TGT C-3′; FOXG1 forward: 5′-AGG AGG GCG AGA AGA AGA AC-3′, reverse: 5′-TGA ACT CGT AGA TGC CGT TG-3′; ISL1 forward: 5′-GCT TTG TTA GGG ATG GGA AA-3′, reverse: 5′-ACT CGA TGT GAT ACA CCT TGG A-3′; TBR1 forward: 5′-GAC TCA GTT CAT CGC CGT CA-3′, reverse: 5′-TCG TGT CAT AAT TAT CCC GAA ATC C-3′; CTIP2 forward: 5′-CAG AGC AGC AAG CTC ACG-3′, reverse: 5′-GGT GCT GTA GAC GCT GAA GG-3′; β-Actin forward: 5′-AAA TCT GGC ACC ACA CCT TC-3′, reverse: 5′-AGA GGC GTA CAG GGA TAG CA-3′.

Statistical analysis

Statistical analysis of data is expressed as means ± standard deviation (SD). *P*-values were calculated using the Student's *t*-test analysis. The statistical significance threshold was set at $*P < 0.05$, $**P < 0.01$ and $***P < 0.001$. Sample sizes are indicated in the figure legends.

Results and discussion

Design and operation of the brain organoids-on-a-chip device

Human brain development *in vivo* is a dynamic and complex process, relying on the coordinated control of inherent cues and the extracellular environment,[30–32] such as the matrix, heterogeneous cell types and mechanical fluid flow (Fig. 1A). The process of hiPSCs-based brain organoids formation *in vitro* often involves stem cell self-renewal, EBs formation and differentiation (Fig. 1B). In this study, we designed an organ-on-a-chip device containing five parallel channels interconnected by micropillar structures (Fig. 1C). In this device, two culture channels permitted 3D culture of EBs by infusing with Matrigel and three medium channels were used for the supply of medium, in which the central medium channel allowed the perfusion of fluid flow. The culture and medium channels were separated from each other by micropillar arrays, which facilitated nutrient and oxygen exchange between the two types of channels. Prior to organoid formation, the suspension of the hiPSCs was seeded in the concave well to form the EBs. After neuroectoderm differentiation of EBs, the mixture of EBs and Matrigel was infused into the culture channels to realize 3D culture in the device. The EBs were immobilized on chip and

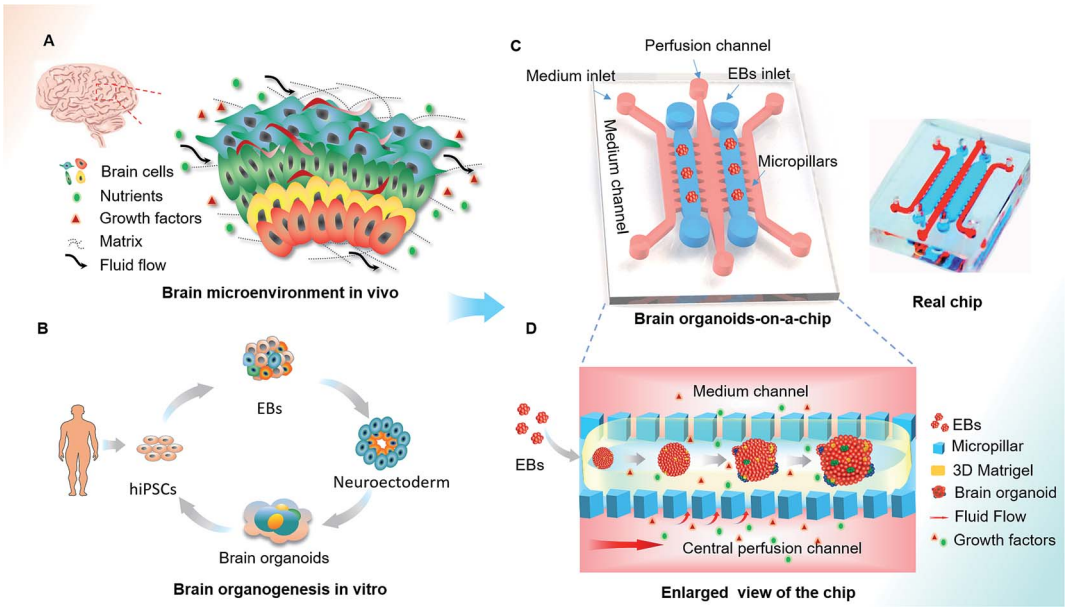

Fig. 1 Schematic diagram of the organ-on-a-chip device for 3D culture and differentiation of brain organoids. (A) The key factors of the brain microenvironment *in vivo*, including fluid flow, extracellular matrix and growth factors. (B) The development process of brain organoids derived from hiPSCs *in vitro*. (C) Configuration of the brain organoids-on-a-chip device. (D) Enlarged view of the procedures for brain organoids generation on the chip. The EBs formed by hiPSCs were embedded in Matrigel and the mixtures were infused into the culture channel. The EBs were differentiated and self-organized into brain organoids in 3D Matrigel under perfused culture conditions.

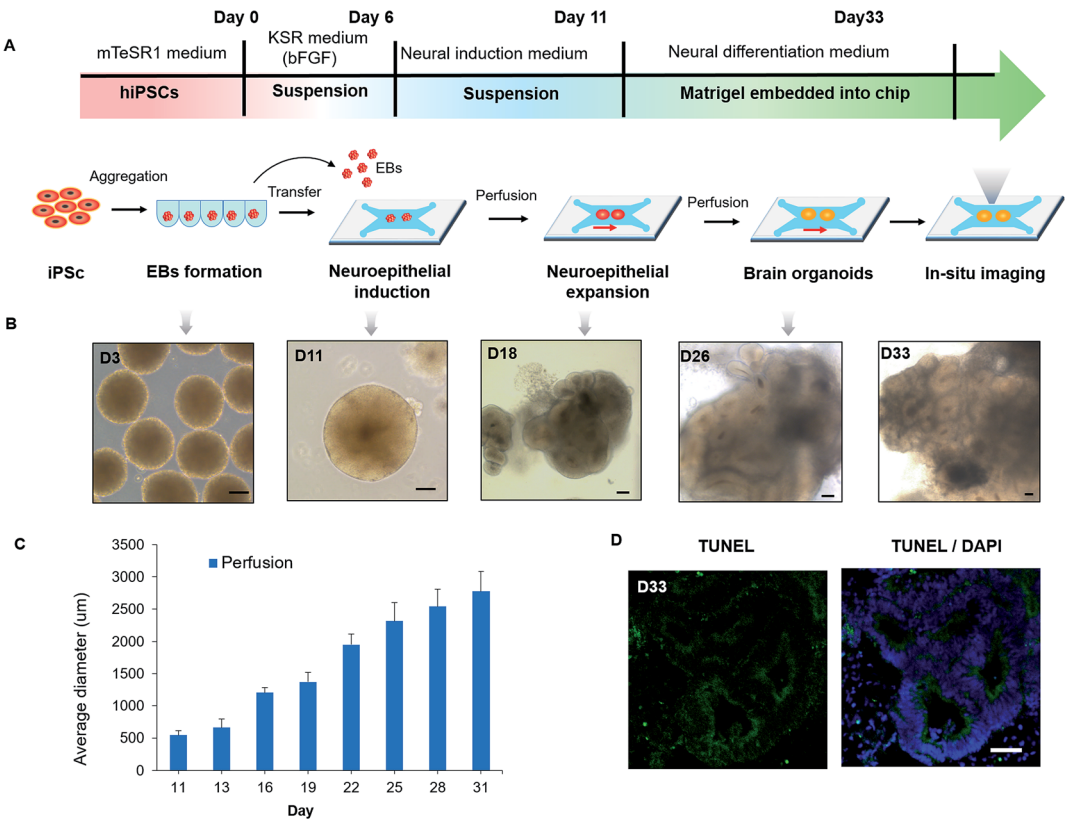

Fig. 2 Characterizing the development of hiPSCs-derived brain organoids in the organ-on-a-chip system. (A) Flow chart of the brain organoid culture and differentiation on a chip. (B) Representative images of cell spheroids taken at different stages. Brain organoids were formed by self-organization and differentiation of the EBs. Scale bars = 100 μm. (C) Size distribution was assessed by the average diameter of brain organoids during the entire course of development under different culture conditions. (D) Frozen sectioning and TUNEL staining for dead cells (green) within brain organoids at day 33. Scale bars = 50 μm.

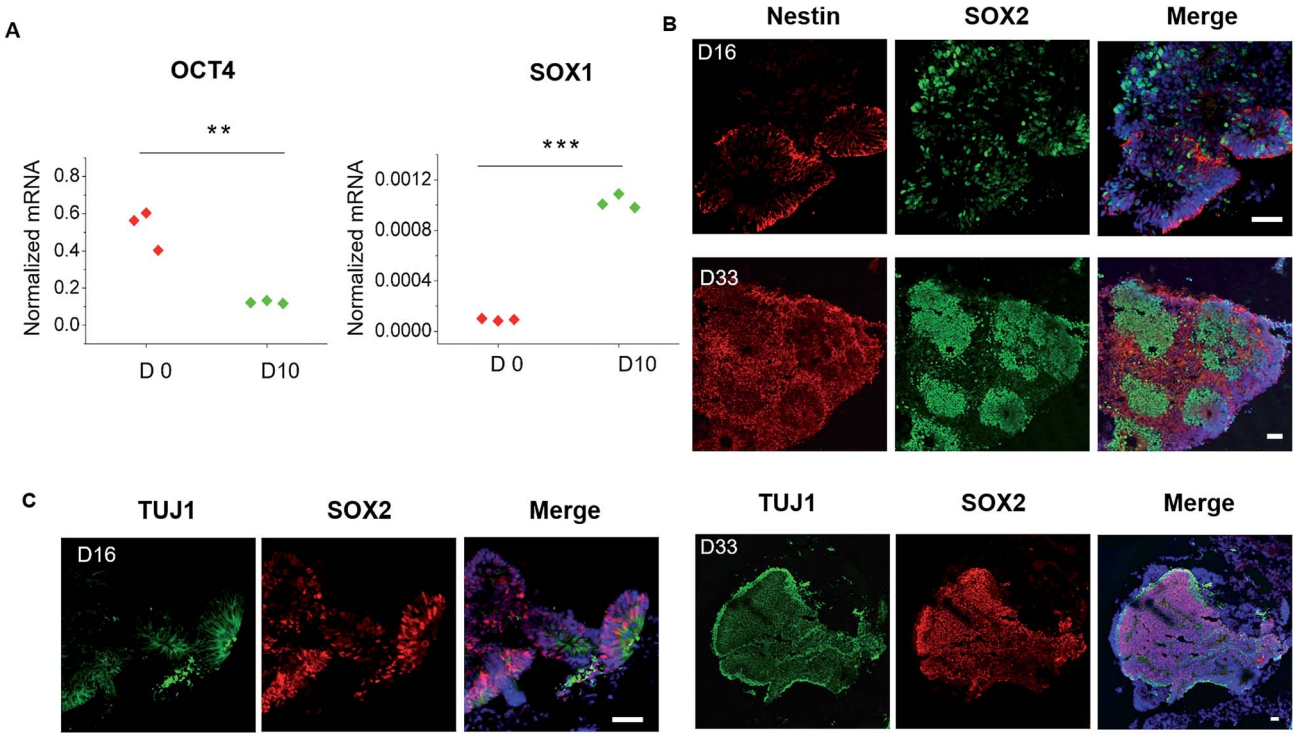

Fig. 3 Examination of neurogenesis in brain organoids generated on chip. (A) Examination of the pluripotent marker OCT4 and neural marker SOX1 in day-0 hiPSCs and day-10 spheroids. The expression values were normalized to the β-actin expression level. Three independent experiments had been performed. Data are shown as mean ± SD. ***$p < 0.001$. (B) Immunohistochemical staining was performed for the neural progenitor markers Nestin and SOX2 in brain organoids after 16 days and 33 days of differentiation. (C) Immunohistochemical staining for neural progenitors (SOX2) and neurons (TUJ1) in organoids at 16 days and 33 days of differentiation.

subsequently *in situ* differentiated into brain organoids (Fig. 1D). In this system, Matrigel as a 3D scaffold plays an essential role in regulating the distribution of nutrient, gases and soluble factors to support the differentiation of stem cells due to its complex components and porous structure.

The continuous flow of medium in the central channel allowed nutrients across the gel channel by diffusion. To evaluate the features of nutrient diffusion under different culture conditions, we used the hydrophilic sodium fluorescein (NaFI, 376 Da) as a tracer and examined its diffusion ability across the

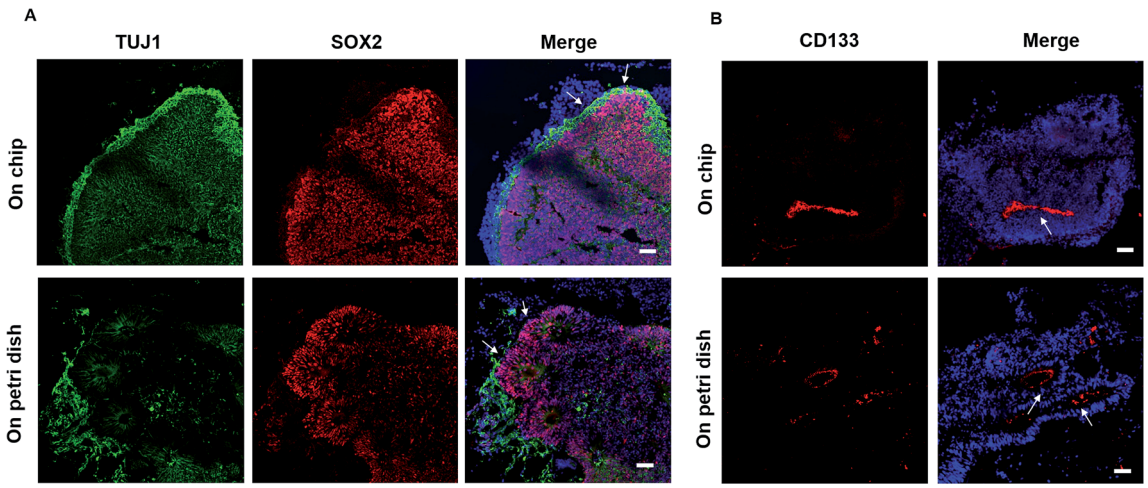

Fig. 4 Comparison of neurogenesis and tissue morphology in brain organoids generated on chip and Petri dish. (A) Examination of TUJ1 and SOX2 markers in 33 day organoids (indicated by arrows) on chip and on Petri dish by immunohistochemical staining. (B) The apical marker CD133 expressed in organoids (indicated by arrows) on chip and on Petri dish at day 33 was verified by immunohistochemical staining, respectively. Scale bars = 50 μm.

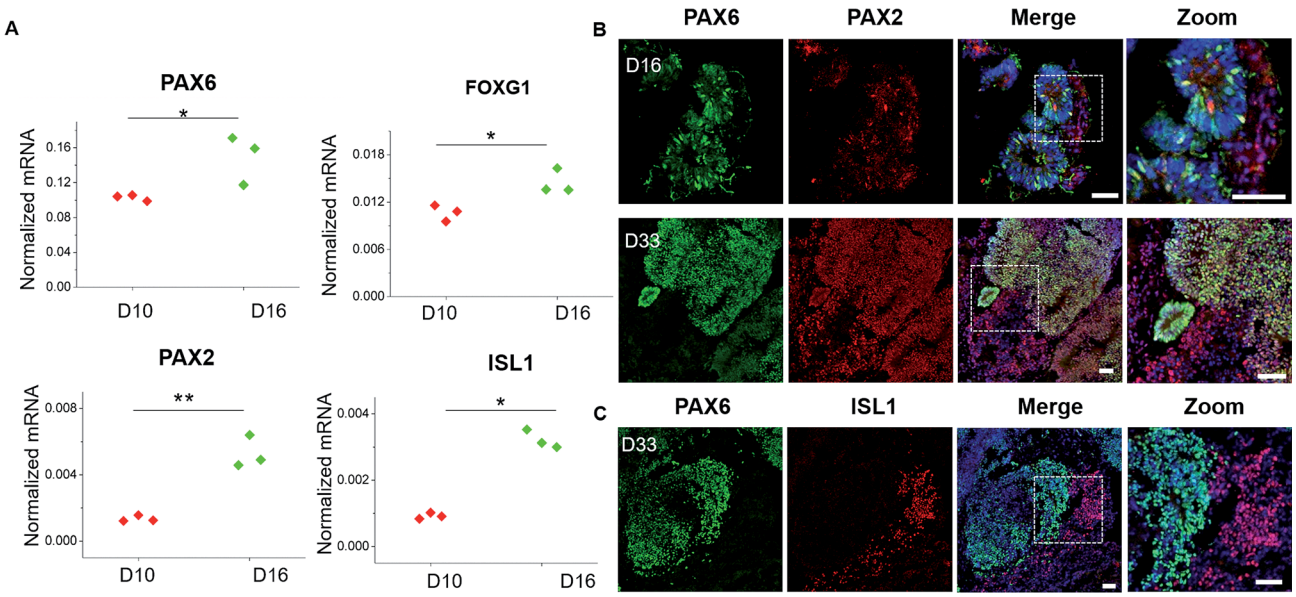

Fig. 5 Identification of specific brain regions in brain organoids. (A) Forebrain markers (PAX6, FOXG1) and hindbrain markers (PAX2, ISL1) were quantified by RT-PCR in spheroids at 10 and 16 days of differentiation. The expression values were normalized to the β-actin expression level. Three independent experiments had been performed. Data are shown as mean ± SD. *$p < 0.05$, **$p < 0.01$. (B) Immunohistochemical staining of PAX6 and PAX2 markers in cryosections of spheroids at 16 days and 33 days. (C) Immunohistochemical staining of PAX6 and ISL1 markers in cryosections of brain organoids at 33 days. Scale bars = 50 μm.

gel channel. The fluorescent tracer was delivered into the central medium channel at a lower rate of 25 μl h^{-1}, and the diffused substances were imaged in the gel channel at different time points. The time-lapse images of fluoresce and intensity profiles showed that the diffusion rate of fluorescein was significantly enhanced over time under perfused culture conditions (ESI Fig. S2A, and S2B†). These data indicate that the presence of fluid flow could potentially facilitate the exchange of soluble substances in this system. In addition, the generated brain organoids exhibited more prominent cell viability under perfused cultures compared to static cultures on chip by TUNEL assay at day 16 and 33. Notably, quantitative analysis showed extensive cell death (about 40% of the TUNEL positive cells) within organoids at day 33 under static cultures, indicating that the perfusion culture could improve cell viability by reducing cell death at the center of organoids with sufficient nutrient supply (ESI Fig. S2C and S2D†). Overall, these results demonstrate that the brain organoids-on-a-chip system incorporated 3D ECM, fluid flow with heterogeneous tissue offers a biomimetic microenvironment to support prolonged culture and generation of brain organoids.

Evaluation of brain organoids growth on chip

The developmental process of brain organogenesis *in vitro* involves the EBs formation, neuroepithelial induction and expansion. To assess the growth of brain organoids in the organ-on-a-chip system, we tested the tissue morphology and viability during the whole period. After the formation of EBs from the hiPSCs, EBs were floating cultured in the ultralow-attached well plate and differentiated into neuroectoderm in neural induction medium (NIM). Then the neuroectoderm tissues were encapsulated in Matrigel to form a mixture and transferred into the culture channels of the chip. After stationary culture for 6–8 hours, the mixture of the EBs and Matrigel was cultured under continuous perfusion conditions for 5–22 days (Fig. 2A). Notably, EBs immobilized within Matrigel on chip were beneficial for *in situ* tracking during organogenesis, which overcame the limitations of imaging in existing protocols. By *in situ* imaging, the neuroepithelial populations were formed in tissues at 15–20 days and expanded to large rosette-like structures in neural differentiation medium (NDM). Finally, the neuroepithelial spheroids were rapidly developed into large and complex brain organoids (Fig. 2B). Fig. 2C showed the size distribution of organoids grown from day 11 to day 31. The average size of organoids was increased due to neuroepithelial differentiation and expansion over time. On day 31, the average diameter of organoids can grow up to about 3 mm. In addition, minimized cell death was observed in the core of brain organoids by TUNEL assay, indicating the improved cell viability in organoids under perfusion culture conditions (Fig. 2D). According to previous reports, the low level of fluid flow was existed in the interstitial space of brain, which has been found to play an important role in supporting neural differentiation and morphogenesis.[33,34] Our results further support that the presence of fluid flow could facilitate the proliferation and differentiation of neural progenitors, which might lead to an increased size of organoids. The gross analysis demonstrate the efficient growth of 3D brain organoid in the biomimetic cellular microenvironment provided by this system, involving EBs formation, cell differentiation and organization of brain organoids.

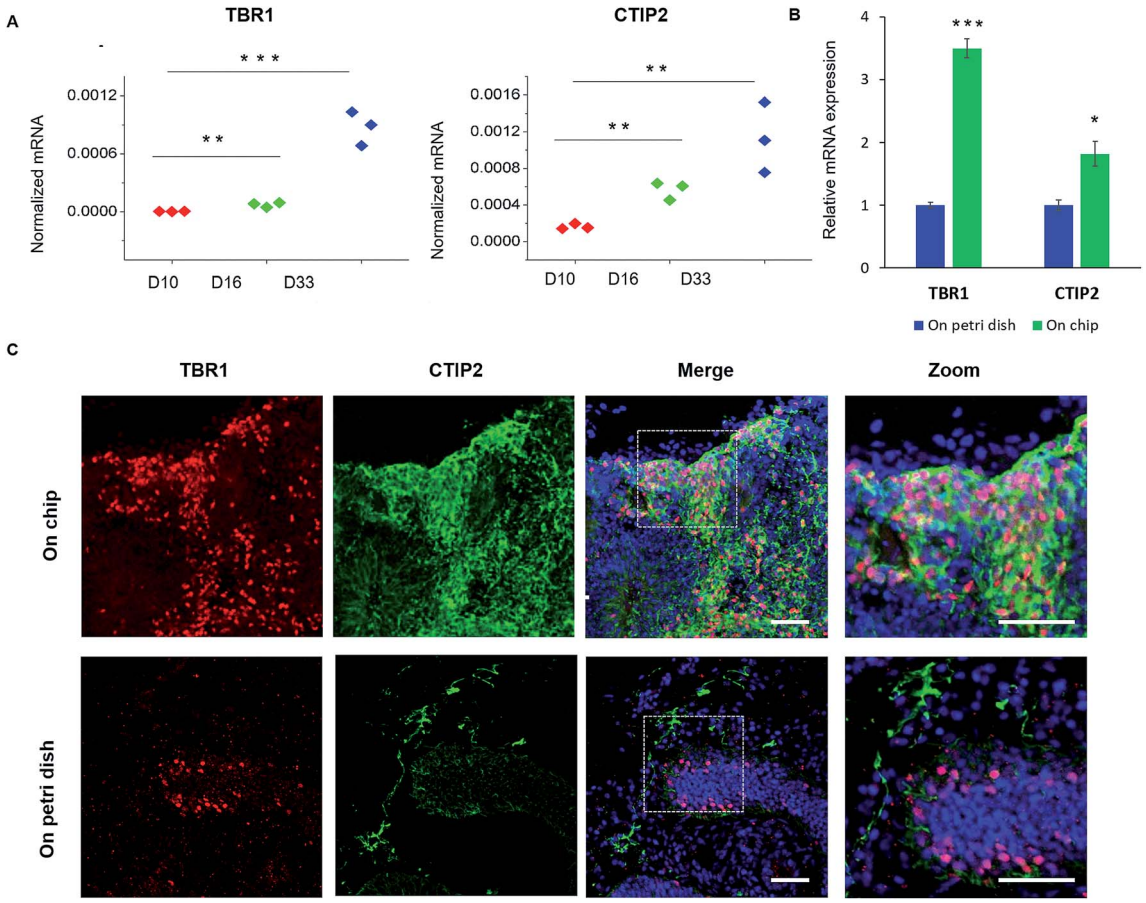

Fig. 6 Spatial organization of cortical neuron subtypes of brain organoids on chip. (A) Relative mRNA expression of pre-plate (TBR1) and deep-layer (CTIP2) markers in spheroids at 10, 16, and 33 days of differentiation. (B) Quantitative comparison of expression levels of cortical neuronal markers in 33 day organoids on chip and Petri dish by RT-PCR. The expression values were normalized to the β-actin expression level. Three independent experiments had been performed. Data are shown as mean ± SD, $*p < 0.05$. $**p < 0.01$, $***p < 0.001$. (C) Immunohistochemical staining for the preplate specific marker TBR1 (red) and the early-born neuron specific marker CTIP2 (green) in brain organoids generated on chip and Petri dish at 33 days, respectively. Scale bars = 50 μm.

Identification of neurogenesis in brain organoids

To evaluate the detailed characterizations of neurogenesis during the course of brain organoid development, we initially examined the efficiency of the early neural induction by performing real-time PCR for specific markers of pluripotent and neural lineage (Fig. 3A). As expected, the expression of pluripotent marker OCT4 was decreased at day 10 of organoids differentiation relative to the control of hiPSCs at day 0, whereas the neural marker SOX1 was significantly upregulated. These data indicate the valid neuroepithelial induction in organoids at early stages. The neural progenitors (Nestin, SOX2) and neuron (TUJ1) markers were further identified in brain organoids at distinct developmental stages. Consistently, high proportions of positive cells for Nestin, SOX2 and TUJ1 were expressed in brain organoids at day 16, even after prolonged development of organoids at day 33 (Fig. 3B). Moreover, immunohistochemical analysis revealed complex heterogeneous regions including SOX2 positive progenitors and TUJ1 positive neurons with large contiguous configurations in 33 day organoids, resemble to the ventricular-like zones. As compared with conventional Petri dish cultures for brain organoids formation, the organoids generated on chip revealed larger and more continuous neuronal organization (ESI Fig. S3† and 4A). Furthermore, the apical marker CD133 was identified in the inner areas of organoids at day 33 (Fig. 4B). It appears that the fluid-filled cavities with a proper apicobasal orientation was formed, reminiscent of brain ventricles. It is noteworthy that these organoids exhibited larger cavities of apical marker CD133 than that cultured on Petri dish (Fig. 4B). Overall, these results suggest the feasibility of brain organoids generated on chip with efficient neural progenitor differentiation and neuronal induction. Our results are consistent with neurogenesis in the brain as they occur during early gestation.

Examination of defined brain regions and cortical organization

Brain development *in vivo* exhibits an orderly sequence of processes, involving the radial organization of progenitor zones and neuronal migration to form distinct brain regions and hierarchical cortical structure.[35–37] Therefore, we further

examined the detailed features of specific brain regions and cortex identities from these generated brain organoids. Brain regionalization at early stages was evaluated by examining the expression of forebrain (PAX6 and FOXG1) and hindbrain (PAX2, ISL1) markers at day 10 and day 16 of organoids differentiation (Fig. 5A). These genes were remarkably upregulated, indicating the presence of both forebrain and hindbrain cell populations. To determine the localization and distribution of these brain region identities within brain organoids, immunohistochemical analysis for the specific markers of forebrain (PAX6) and hindbrain (PAX2, ISL1) was performed (Fig. 5B and C). The high expression of PAX6 and PAX2 positive populations were observed in brain organoids at day 16, which was consistent with genes expression. As development proceeded, the organoids displayed increasing refinement of brain region specification at day 33, indicating the developmental expansion of brain organoids. In addition, the PAX2 or ISL1 positive regions were expressed either overlapped or discrete located to PAX6 regions, implying the probably rudimentary definition of brain regions as displayed *in vivo*. These results reveal the proper differentiation of discrete and independent brain regions identities in organoids grown on chip.

To further study the features of cortical organization, we initially analyzed the expression of relative genes, including preplate marker TBR1 and deep-layer neuron marker CTIP2 (Fig. 6A). The expression of these genes significantly increased during the developmental stages of brain organoids from day 10 to day 33. Furthermore, the cortex structure was identified by immunohistochemical staining for cortical neuronal subtypes (TBR1 and CTIP2) in organoids at day 33. As shown in Fig. 6C, organoids displayed high expression of TBR1 and CTIP2 along the peripheral of tissue, suggesting the formation of the initial cortex containing basal neural layer and deep neural layers. Meanwhile, the CTIP2 neurons appeared to be adjacent to the TBR1 preplate and located in the internal side, which might reveal a rudimentary spatial organization of cortical neuronal layers as the brain organoids developed. Notably, organoids displayed more increased expression of cortical markers (TBR1 and CTIP2) and more defined organization of cortical neurons on chip than that on Petri dish (Fig. 6B and C). These differences between two organoid models suggest that the chip perfusion system enhanced cortical neurons differentiation and improved cortex organization in brain organoid compared with Petri dish cultures, which might further confirm the importance of favorable microenvironment on cortical development in this system. Overall, these results demonstrate that brain organoids generated on chip exhibited essential characteristics of the human early fetal brain. We assume that the biomimetic cellular microenvironment offered by this system may serve as a crucial factor to support the self-organization of hiPSCs into functional brain organoids *in vitro*.

Conclusion

In summary, we presented a new approach to generate 3D brain organoids derived from hiPSCs using a perfusable organ-on-a-chip system. The generated brain organoids displayed favorable growth and specific feature identities including neuronal differentiation, brain regionalization and cortical spatial organization in a biomimetic cellular niche, modeling the early human brain organogenesis *in vivo*. Particularly, the brain organoids cultured in the perfused system showed improved cortical development compared with static cultures on Petri dish. The established brain organoids-on-a-chip device is simple, low-cost and easy to operate, which can not only facilitate long term 3D culture and formation of brain organoids with sufficient nutrients exchange by small volume of medium consumption, but also be amenable to *in situ* tracking and real-time imaging, which partially addresses the potential limitations in conventional methods.

This work provides a proof-of-concept to engineer the hiPSCs-based brain organoids by combining stem cell biology with organs-on-a-chip technology. This approach can be further implemented with additional microfluidic elements to greatly improve the function and maturity of stem cell-derived brain organoids, holding promising applications in developmental biology and disease modeling studies.

Conflicts of interest

The authors have no conflicts of interest to declare.

Acknowledgements

This research was supported by the Strategic Priority Research Program of the Chinese Academy of Sciences (XDA16020900, XDPB0305), National Natural Science Foundation of China (No. 91543121, 31671038, 81573394, 31600784), International Science and Technology Cooperation Program of China (2015DFA00740) and Key Laboratory of Separation Science for Analytical Chemistry (Dalian Institute of Chemical Physics, Chinese Academy of Sciences). We thank Professor Ning Sun (Fudan University, China) for kindly providing the human induced pluripotent stem cells.

References

1 M. A. Lancaster and J. A. Knoblich, *Science*, 2014, **345**, 1247125.
2 H. Clevers, *Cell*, 2016, **165**, 1586–1597.
3 Y. Sasai, *Cell Stem Cell*, 2013, **12**, 520–530.
4 A. Fatehullah, S. H. Tan and N. Barker, *Nat. Cell Biol.*, 2016, **18**, 246–254.
5 G. Quadrato, J. Brown and P. Arlotta, *Nat. Med.*, 2016, **22**, 1220–1228.
6 M. A. Lancaster, M. Renner, C. A. Martin, D. Wenzel, L. S. Bicknell, M. E. Hurles, T. Homfray, J. M. Penninger, A. P. Jackson and J. A. Knoblich, *Nature*, 2013, **501**, 373–379.
7 X. Qian, H. N. Nguyen, M. M. Song, C. Hadiono, S. C. Ogden, C. Hammack, B. Yao, G. R. Hamersky, F. Jacob, C. Zhong, K. J. Yoon, W. Jeang, L. Lin, Y. Li, J. Thakor, D. A. Berg, C. Zhang, E. Kang, M. Chickering, D. Nauen, C. Y. Ho, Z. Wen, K. M. Christian, P. Y. Shi, B. J. Maher, H. Wu,

P. Jin, H. Tang, H. Song and G. L. Ming, *Cell*, 2016, **165**, 1238–1254.
8 T. Takebe, K. Sekine, M. Enomura, H. Koike, M. Kimura, T. Ogaeri, R. R. Zhang, Y. Ueno, Y. W. Zheng, N. Koike, S. Aoyama, Y. Adachi and H. Taniguchi, *Nature*, 2013, **499**, 481–484.
9 S. R. Finkbeiner, X. L. Zeng, B. Utama, R. L. Atmar, N. F. Shroyer and M. K. Estes, *mBio*, 2012, **3**, e00159-12.
10 A. M. Pasca, S. A. Sloan, L. E. Clarke, Y. Tian, C. D. Makinson, N. Huber, C. H. Kim, J. Y. Park, N. A. O'Rourke, K. D. Nguyen, S. J. Smith, J. R. Huguenard, D. H. Geschwind, B. A. Barres and S. P. Pasca, *Nat. Methods*, 2015, **12**, 671–678.
11 M. Eiraku, K. Watanabe, M. Matsuo-Takasaki, M. Kawada, S. Yonemura, M. Matsumura, T. Wataya, A. Nishiyama, K. Muguruma and Y. Sasai, *Cell Stem Cell*, 2008, **3**, 519–532.
12 T. Kadoshima, H. Sakaguchi, T. Nakano, M. Soen, S. Ando, M. Eiraku and Y. Sasai, *Proc. Natl. Acad. Sci. U. S. A.*, 2013, **110**, 20284–20289.
13 M. Jorfi, C. D'Avanzo, D. Y. Kim and D. Irimia, *Adv. Healthcare Mater.*, 2017, 1700723.
14 J. Mariani, M. V. Simonini, D. Palejev, L. Tomasini, G. Coppola, A. M. Szekely, T. L. Horvath and F. M. Vaccarino, *Proc. Natl. Acad. Sci. U. S. A.*, 2012, **109**, 12770–12775.
15 M. A. Lancaster and J. A. Knoblich, *Nat. Protoc.*, 2014, **9**, 2329–2340.
16 H. Kurosawa, *J. Biosci. Bioeng.*, 2007, **103**, 389–398.
17 D. A. Feinberg and A. S. Mark, *Radiology*, 1987, **163**, 793–799.
18 L. Li and T. Xie, *Annu. Rev. Cell Dev. Biol.*, 2005, **21**, 605–631.
19 J. Voog and D. L. Jones, *Cell Stem Cell*, 2010, **6**, 103–115.
20 A. M. Ghaemmaghami, M. J. Hancock, H. Harrington, H. Kaji and A. Khademhosseini, *Drug Discovery Today*, 2012, **17**, 173–181.
21 A. D. van der Meer and A. van den Berg, *Integr. Biol.*, 2012, **4**, 461–470.
22 S. N. Bhatia and D. E. Ingber, *Nat. Biotechnol.*, 2014, **32**, 760–772.
23 M. Chung, S. Lee, B. J. Lee, K. Son, N. L. Jeon and J. H. Kim, *Adv. Healthcare Mater.*, 2017, 1700028.
24 D. Huh, B. D. Matthews, A. Mammoto, M. Montoya-Zavala, H. Y. Hsin and D. E. Ingber, *Science*, 2010, **328**, 1662–1668.
25 A. Schepers, C. Li, A. Chhabra, B. T. Seney and S. Bhatia, *Lab Chip*, 2016, **16**, 2644–2653.
26 H. J. Kim, D. Huh, G. Hamilton and D. E. Ingber, *Lab Chip*, 2012, **12**, 2165–2174.
27 J. M. Peyrin, B. Deleglise, L. Saias, M. Vignes, P. Gougis, S. Magnifico, S. Betuing, M. Pietri, J. Caboche, P. Vanhoutte, J. L. Viovy and B. Brugg, *Lab Chip*, 2011, **11**, 3663–3673.
28 Y. K. Kurokawa, R. T. Yin, M. R. Shang, V. S. Shirure, M. L. Moya and S. C. George, *Tissue Eng., Part C*, 2017, **23**, 474–484.
29 S. Takeuchi, Y. Nishida and T. Mizushima, *Journal of Physical Therapy Science*, 2015, **27**, 1819–1822.
30 N. J. Abbott, *Neurochem. Int.*, 2004, **45**, 545–552.
31 J. M. Rutkowski and M. A. Swartz, *Trends Cell Biol.*, 2007, **17**, 44–50.
32 M. A. Swartz and M. E. Fleury, *Annu. Rev. Biomed. Eng.*, 2007, **9**, 229–256.
33 M. E. Desmond and A. G. Jacobson, *Dev. Biol.*, 1977, **57**, 188–198.
34 J. A. Miyan, M. Nabiyouni and M. Zendah, *Can. J. Physiol. Pharmacol.*, 2003, **81**, 317–328.
35 Z. Molnar and A. Pollen, *Development*, 2014, **141**, 11–16.
36 I. H. Smart, C. Dehay, P. Giroud, M. Berland and H. Kennedy, *Cereb. Cortex*, 2002, **12**, 37–53.
37 L. H. Tsai and J. G. Gleeson, *Neuron*, 2005, **46**, 383–388.